THE JOURNAL OF PHYSICAL CHEMISTRY C

Article

pubs.acs.org/JPCC

Direct Imaging of Hydrogen Bond Formation in Dissociative Adsorption of Glycine on Si(111)7×7 by Scanning Tunneling Microscopy

A. Chatterjee, L. Zhang, and K. T. Leung*

WATLab and Department of Chemistry, University of Waterloo, Waterloo, Ontario N2L 3G1, Canada

ABSTRACT: Adsorption of glycine on a Si(111)7×7 surface at room temperature has been studied by scanning tunneling microscopy (STM). The observed STM images provide strong evidence for dissociative adsorption of glycine through N−H bond cleavage (and N−Si bond formation) as reported in our recent X-ray photoemission study. In particular, the dissociated H atom is found to anchor on a restatom while the N−H dissociated glycine molecule adsorbs on an adatom in a tilted, unidentate geometry. STM study for higher exposures further reveals that the second adlayer is mediated by vertical hydrogen bonding, in excellent accord with our recent X-ray photoemission results. In addition to this vertical hydrogen bonding between a glycine molecule and the N−H dissociated glycine adsorbate, we also observe horizontal hydrogen bonding, not seen before, between two N−H dissociated glycine adsorbates at two neighboring adatom sites. These hydrogen-bonded adstructures, as implicated in the STM images, have been corroborated with our computational DFT/B3LYP/6-31++(d,p) results by using the two largest model surfaces: a $Si_{16}H_{18}$ cluster to simulate an adatom−restatom pair and a $Si_{26}H_{24}$ cluster to model a double adatom−adatom pair across the dimer wall of the 7×7 surface. Furthermore, statistical analysis of the STM images for different exposures shows that the center adatom is more reactive than the corner adatom and that the faulted half is more reactive than the unfaulted half. The horizontal hydrogen bonding appears to be favored at a lower exposure than the vertical hydrogen bonding, which becomes dominant at a higher exposure as formation of the second adlayer proceeds. The present work illustrates the importance of hydrogen bonding in the early growth and site-specific chemistry of glycine on Si(111)7×7 surfaces.

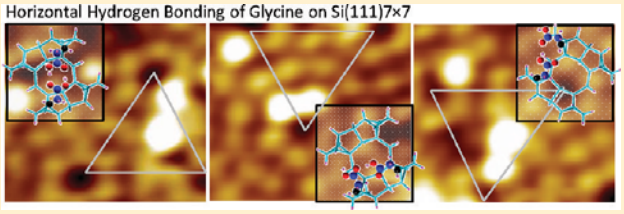

1. INTRODUCTION

There is a lot of interest in the interactions and surface chemistry of organic and biological molecules, including, for example, amino acids, proteins, peptides, nucleosides, DNA, and RNA, on a variety of metal[1−3] and semiconductor[4−6] substrates.[7,8] Understanding the nature of molecule-to-molecule and molecule-to-substrate interactions is very important for developing chemical sensors,[9] molecular devices,[10,11] biomolecular electronic components,[12,13] and emerging nanotechnology applications.[14] Among the semiconductor substrates, Si(111)7×7 represents one of the most studied surfaces and offers a variety of bonding sites to approaching bio/organic adsorbates. Different organic molecules with different functional groups, including acetic acid,[15] benzene,[16] pyrrole,[17] methanol,[18] butadiene,[19] dimethyl- and trimethylamines,[20] and glycine,[5,21] on Si(111)7×7 have been found to undergo different types of reactions with the surface upon adsorption. For example, benzene[16] and butadiene[19] adsorb on the 7×7 surface through the cycloaddition reaction, while pyrrole[17] and methanol[18] undergo H dissociative adsorption. Furthermore, the carboxylic acids and the amines are especially interesting because their reaction mechanisms are quite different on the 7×7 surface. For carboxylic acids (e.g., acetic acid[15]), H dissociative adsorption is found to produce a conjugate base with the formation of an O−Si bond, although its mechanism is far from well understood. For amines,[20] there has been evidence to support the formation of stable, datively bonded surface adducts by partially donating the lone pair electron density of the N atoms toward the Si atoms. One particularly interesting question is the relative reactivity of the carboxylic acid group and the amino group toward the 7×7 surface. The amino acids therefore offer such a unique testing ground because they are bifunctional molecules with both the acidic (carboxylic acid group) and basic (amino group) moieties.

The amino acids are also the smallest building blocks of proteins and peptides and are capable of forming hydrogen bonding. Among the ten naturally occurring amino acids that are produced by the human body, glycine is structurally the simplest one, making it an excellent starting point to study specific interactions between the amino and carboxylic acid groups and with the substrate bonding sites. To date, there are only a few studies on glycine adsorption on Si(111)7×7 and Si(100)2×1. In particular, Lopez et al. studied glycine adsorption on Si(100)2×1 by high-resolution electron energy loss spectroscopy (HREELS) and reported an unidentate adstructure obtained by O−H dissociative adsorption and the formation of O−Si bond.[22] Later, Qu et al. showed in a computational study that O−Si bond formation is preferred

Received: January 1, 2012
Revised: April 24, 2012
Published: May 11, 2012

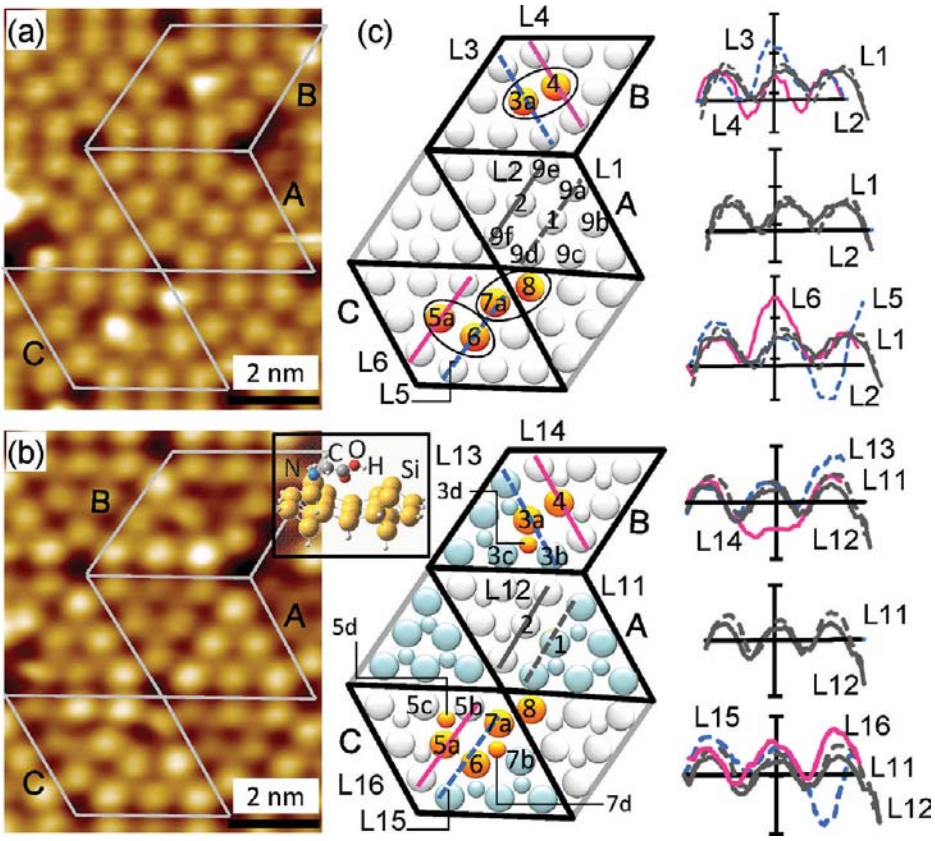

Figure 1. (a) STM empty-state image and (b) filled-state image of glycine adsorbed on Si(111)7×7 surface obtained with sample bias of +2 and −2 V, respectively, all at a tunneling current of 200 pA. (c) Schematic drawings (center column) of three 7×7 unit cells labeled A, B, and C for the STM images, and height profiles (right column) along linescan L*x* (*x* = 1−6, 11−16) in the unfaulted half (marked by solid lines) and faulted half (marked by dashed lines). The atoms in the unfaulted and faulted half unit cells are represented by lighter and darker spheres, respectively, in the lower part of panel c. The sites of interest are labeled by alphanumeric characters. The ovals in the upper part of panel c mark the adatom−adatom pairs across the dimer wall that are affected by glycine adsorption. The inset in panel c shows the equilibrium geometry of a N−H dissociated glycine molecule adsorbed on a $Si_{26}H_{24}$ cluster in a tilted configuration as obtained by DFT/B3LYP/6-31++G(d,p) calculation.

over N−Si bond formation on Si(100)2×1, both thermodynamically and kinetically.[23] For glycine adsorption on Si(111)-7×7, Huang et al. studied multilayer growth by X-ray photoelectron spectroscopy (XPS) and HREELS.[5] They concluded that glycine adsorbs, via dissociation of both N−H and O−H bonds, in a bidentate configuration through the formation of N−Si and O−Si bonds with two Si adatoms. However, the glycine molecule with a NH_2−OH separation of 3.7 Å appears to be physically much too small to realize the proposed bidentate structure that bridges across two adjacent adatoms, with a separation of 6.65 Å. In our recent XPS investigation of glycine on Si(111)7×7,[21] we demonstrate that glycine adsorbs in an unidentate configuration through N−H dissociation with the carboxylic acid group remaining intact. With increasing exposure, we also observe the formation of a hydrogen-bonded intermediate layer and its evolution to zwitterionic multilayer. This observation is supported by our recent computational study, which shows that the formation of a Si←N adduct leads to unidentate N−H dissociative adproduct on a model Si(111)7×7 surface, in contrast to that found on a model Si(100)2×1 surface, where Si←O adduct formation leads to unidentate O−H dissociative adproduct.[24] There are also rather limited studies of glycine on metal surfaces, all of which show evidence of hydrogen bonding. In particular, self-assembly of glycine on Cu{110} surfaces has been studied by Chen et al. using scanning tunneling microscopy (STM) to show the presence of hydrogen bonding in two different domains on the surface.[3] In a separate study, Nyberg et al. demonstrated the formation of hydrogen bonds between the deprotonated glycine molecules (in the form of glycinate) on a Cu(110) surface by X-ray emission spectroscopy and near-edge X-ray absorption fine structure methods, along with theoretical simulations.[25]

The Si(111)7×7 surface offers a set of unique, directional bonding sites to approaching molecules.[26] The 7×7 unit cell consists of 12 adatoms in the first layer, 6 restatoms in the second layer, and the 1 corner hole in the third layer, which together give 19 dangling bonds.[25] Charge transfer from a restatom to an adatom results in a formal charge of $+^{7}/_{12}$ for the electrophilic adatom and −1 for the nucleophilic restatom.[27,28] Because a corner (angulus in Latin) adatom (AA) has only one neighboring restatom (RA) while a center (centrum in Latin) adatom (CA) has two neighboring RAs, almost twice the amount of charge transfer from CA to RA as that from AA to RA occurs, therefore causing the CA to have a larger formal charge than AA. The differences in the formal charges of CA (∼+1), AA ($+^{7}/_{12}$), and RA (−1) contribute to their site-specific reactivities. The availability of both the nucleophilic and electrophilic sites makes the 7×7 surface particularly interesting toward various organic adsorbates with

dx.doi.org/10.1021/jp300011k | J. Phys. Chem. C 2012, 116, 10968−10975

different functional groups. For small organic molecules such as glycine (with the NH_2−OH separation of 3.7 Å for the most stable conformer in the isolated gaseous state), the neighboring adatom−restatom pairs (CA−RA or AA−RA, with a separation of 4.57 Å) represent the most important reaction sites. This is because of their generally similar and therefore physically compatible dimensions, in contrast to the considerably larger separations for CA−CA pair across the dimer wall (6.65 Å), CA−CA pair within a half unit cell (7.68 Å), CA−AA within a half unit cell (7.68 Å), and CA−AA across the dimer wall pairs (10.15 Å). For example, dissociative adsorption of pyrrole and amines on the CA and AA sites[16,19] and cycloaddition reactions of thiophene and cyclohexadienes (1,3 and 1,4) on the adjacent adatom−restatom pairs[29,30] of Si(111)7×7 have been reported.

In the present work, we investigate the adsorption of glycine on the Si(111)7×7 surface at room temperature and report the first STM images of this fundamentally important system. Of particular interest are the interactions of the amino and carboxylic acid groups in glycine with different bonding sites (CA, AA, RA) on the 7×7 surface and their site-specific chemistry. The present results illustrate, for the first time, the importance of hydrogen bonding in a variety of adsorption configurations for the growth evolution of glycine on a semiconductor surface.

2. EXPERIMENTAL DETAILS

All the experiments were performed in a five-chamber, multitechnique ultrahigh vacuum system (Omicron Nanotechnology Inc.) with a base pressure of 7×10^{-11} mbar. The analysis chamber was equipped with an X-ray photoelectron spectrometer (with a SPHERA analyzer and a seven-channel detector), a monochromatic Al Kα source, and a variable-temperature scanning probe microscope (VT-SPM, with Matrix V2.1 software). An electrochemically etched, atomically sharp W tip was used for the STM measurement conducted at room temperature. A 11×2 mm^2 substrate was cut from a single-side polished, n-type As-doped Si(111) wafer (0.3 mm thick) with a resistivity of 0.005 Ω cm (Virginia Semiconductors). The Si(111) substrate could be heated by passing a direct current and was precleaned by thoroughly outgassing at 400 °C overnight (in the analysis chamber). The 7×7 reconstruction could be routinely generated by flash-annealing the freshly outgassed substrate at ∼1200 °C for 5 s and rapid cooling to 800 °C, followed by slow cooling (at 4−5 °C/s) to room temperature. The cleanliness of the surface was verified by sharp STM images of large-area, contaminant-free terraces of the 7×7 unit cells, with a low surface defect concentration <1%. The clean 7×7 substrate was then transferred into the organic deposition chamber (with a base pressure of 2×10^{-10} mbar) and was dosed with glycine by using a low-temperature organic material effusion cell (Dr. Ebert MBE-Komponenten GmbH). The amount of glycine exposed to the 7×7 substrate was controlled by the exposure time with the effusion cell operating at 120 °C and the deposition chamber pressure at 1×10^{-9} mbar.[21] The purity of glycine during its exposure to the 7×7 substrate was verified by collecting its mass spectrum in situ with a quadrupole mass spectrometer (Stanford Research Systems RGA-300). After exposure, the sample was transferred back to the analysis chamber for STM imaging in constant current mode. During STM measurements, the pressure in the analysis chamber was never above 2×10^{-10} mbar.

3. RESULTS AND DISCUSSION

Parts a and b of Figure 1 show the STM images of Si(111)7×7 after a 20 s exposure of glycine obtained with a tunneling current of 200 pA at a sample bias of +2 and −2 V, corresponding to empty-state and filled-state imaging, respectively. In Figure 1c, we show the corresponding schematic diagrams of three 7×7 unit cells (labeled A, B, and C) with representative features attributable to glycine adsorption, and we identify specific CA, AA, or RA sites with alphanumeric labels. The empty-state image (Figure 1a) for cell A shows the local density of states (LDOS) of the unreacted or pristine 7×7 unit cell of the Si(111) surface, in which all the adatoms in both the faulted and unfaulted half unit cells exhibit similar intensities, as reflected also by the corresponding height profiles along the edges of the half unit cells (line scans L1 and L2, Figure 1c upper). Unless stated otherwise, all the height profiles correspond to line scans starting from left to right of images. In the corresponding filled-state image (Figure 1b), the six spheres representing the adatoms in the faulted half A (shaded spheres in Figure 1c lower) appear brighter than those in the unfaulted half A (unshaded spheres in Figure 1c lower). In the filled-state image (Figure 1b), we can also identify the LDOS surrounded by three neighboring adatoms as the restatoms (smaller circles in Figure 1c lower). The height profile along line scan L11 across the three adatoms in the faulted half shows the similarity of LDOS of these adatoms. The maximum height differential between L11 (for the faulted half) and its corresponding line scan L12 for the unfaulted half (Figure 1c lower) is found to be larger by 1 Å. In contrast, there is no difference in the maximum height differential between L1 and L2 (Figure 1c upper) in the empty-state image. These observations are in excellent accord with earlier STM work for the pristine Si(111)7×7 surface.[31]

In the empty-state image (Figure 1a), the faulted half unit cell B depicts a brighter oblong protrusion located closer to a dimer wall from the CA3a site (Figure 1c, upper), which indicates the adsorption of a glycine moiety. The protrusion is particularly evident in the height profile along line scan L3, which shows a larger density than the corresponding unreacted sites along reference line scan L1. The presence of the adsorbed glycine moiety also appears to affect the LDOS of the CA4 site on the complementary (unfaulted) half unit cell B, as shown in the corresponding height profile along line scan L4. On the other hand, in the filled-state image (Figure 1b), the reacted CA3a in the faulted half unit cell B appears to be nearly as bright as the unreacted CA1 in the faulted half unit cell A but with the centroid shifted toward the dimer wall. Interestingly, glycine adsorption at the CA3a site also depletes the LDOS at the CA4 site in the unfaulted half unit cell B across the dimer wall. These LDOS variations are clearly depicted in the height profiles along the respective line scans L13 and L14. In addition, there is no discernible density at the restatom RA3d site next to the reacted CA3a site, while the LDOS of the two adjacent adatoms AA3b and CA3c appear to increase. As reported earlier[32,33] and discussed further below, these LDOS changes are the signature of H adsorption at the restatom, which therefore indicates that glycine adsorption at CA3a produces a dissociated H atom that adsorbs at the RA3d site.

Our recent XPS study[21] has shown that glycine adsorbs on Si(111)7×7 in a unidentate fashion by N−H dissociation with the formation of a N−Si bond, and no evidence of bidentate adsorption is found. In particular, one adatom−restatom pair is

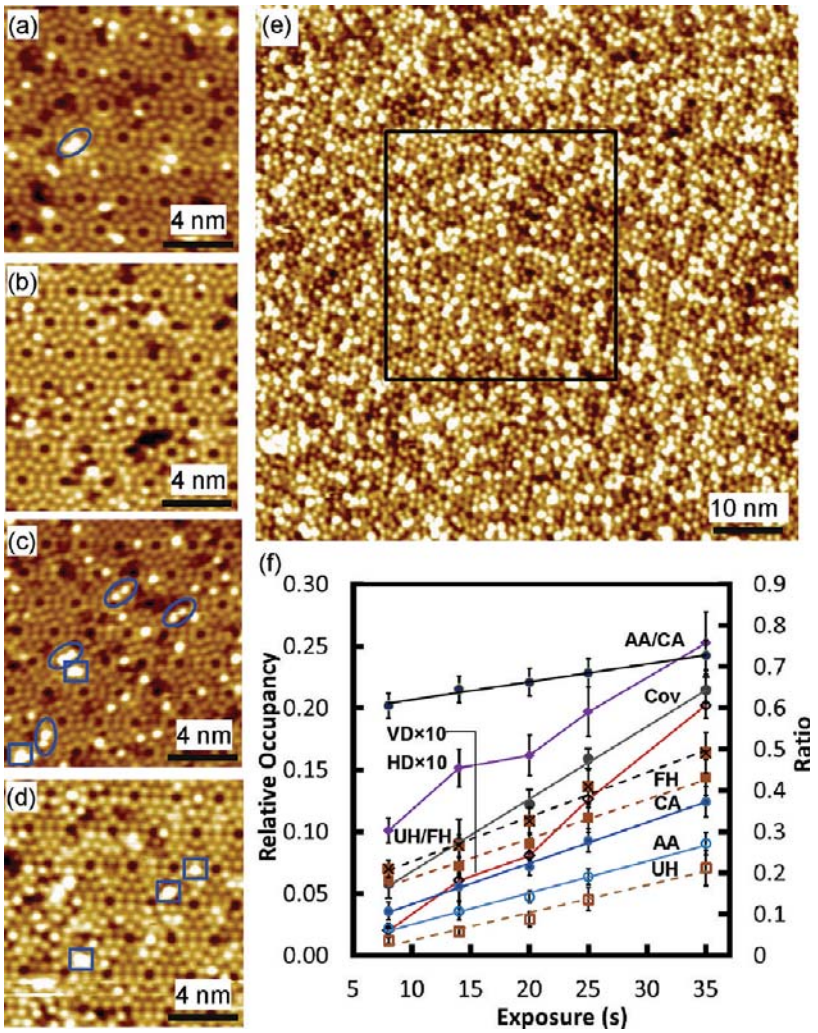

Figure 2. STM images taken at a sample bias of +2 V and a tunneling current of 200 pA after glycine exposure of (a) 8 s, (b) 14 s, (c) 20 s, (d) 25 s, and (e) 35 s and (f) the corresponding total coverage (Cov) and the relative occupancies for center adatom (CA), corner adatom (AA), faulted half (FH), and unfaulted half (UH) sites and for vertical doubles (VD) and horizontal doubles (HD). The ratios of AA to CA and UH to FH are shown on the right axis.

involved in the reaction with glycine, with the N−H dissociative glycine fragment, $-NHCH_2COOH$, and the dissociated H atom adsorbed onto the adatom and restatom, respectively. We have not considered the adsorption of the dissociated H atom on another adatom because Lo et al. reported that H adsorption is energetically more favorable on the restatom than on the adatom.[34] Our model is consistent with the observed LDOS changes of the CA3a and RA3d pair in the filled-state image (Figure 1b), in which H adsorption at RA3d, as reflected by the density depletion, causes an electron redistribution that increases the density of the two adjacent unreacted adatoms, AA3b and CA3c. Similar correlated bright-dark STM features as observed for the adatom−restatom pair in the present work have also been reported in the literature.[16,19,31−33] For instance, in their combined STM−XPS study of adsorption of secondary and tertiary amines on Si(111)7×7,[19] Cao et al. observed correlated bright-dark features for dimethylamine but only bright protrusions for trimethylamine on Si(111)7×7. They concluded that the dark regions correspond to the adsorption of dissociated H atoms from dimethylamine on the restatoms next to the adsorbed dimethylamine moiety on the adatom, and the lack of dark regions in the STM image for the case of trimethylamine (which contains only methyl H atoms and therefore does not undergo H dissociation) supports the aforementioned assignment.

The LDOS of the center adatom across the dimer wall, CA4, from the reacted adatom CA3a is also found to be dramatically reduced in the filled-state image (Figure 1c, lower, L14) and narrower in the empty-state image (Figure 1c upper, L4), when compared to those across the unreacted site CA2 (corresponding to L12 and L2, respectively). This suggests interactions between the adsorbed glycine fragment at CA3a and the adatom CA4. In our recent computational study using density functional theory calculations with a 6-31G++(d,p) basis set,[23] we consider only vertical unidentate adstructure at the adatom−restatom pair. Given the observed STM image (Figure 1b), we have now extended our calculations to include a near-horizontal unidentate adstructure tilted across the dimer wall, as modeled by a $Si_{26}H_{24}$ cluster discussed below. The tilted adstructure for the N−H dissociated glycine molecule, shown as the inset in Figure 1c, is believed to involve some form of

dx.doi.org/10.1021/jp300011k | J. Phys. Chem. C 2012, 116, 10968−10975

"weak" dipole−dipole-like interaction between the "free" terminal −COOH group (with a negative partial charge) and the center adatom across the dimer wall (with a positive partial charge). Considering the difference in the clusters, the adstructure obtained on $Si_{26}H_{24}$ is also found to have an adsorption energy (−348.1 kJ mol^{-1}) more negative than that of the vertical unidentate adstructure obtained on $Si_{16}H_{18}$ (−266.4 kJ mol^{-1}), which confirms the feasibility of such a tilted adstructure. On the other hand, the formation of a stable bidentate adstructure bonded to two adatoms across the dimer wall cannot be realized with the present calculation, likely because the distance between two adatoms (6.65 Å) is too large for a glycine molecule (with the N-to-O separation of 3.70 Å) to form a bidentate product. Furthermore, if there were a bidentate configuration, the dissociated H atom from the −OH group would have adsorbed on one of the neighboring restatoms in the complementary half unit cell B. As all the restatoms in the unfaulted half unit cell B are clearly seen to be unaffected in the filled-state image (Figure 1b), this would confirm the absence of the second dissociated H atom and therefore of the bidentate geometry. In addition, the orientation of the bright protrusion (e.g., CA3a) across the dimer wall (e.g., toward CA4) instead of toward the restatoms in the empty-state image (Figure 1a) also allows us to rule out bidentate configuration across an adatom−restatom pair within the same half unit cell.

In addition to adsorption on the faulted half, as illustrated in unit cell B, the empty-state image for unit cell C shows other adsorption configurations (Figure 1a). In particular, the bright protrusions correspond to adsorption of a glycine molecule at a center adatom CA5a on the unfaulted half and of that at a corner adatom AA7a across the dimer wall on the faulted half (Figure 1a). Evidently, the oblong protrusion at CA5a extending toward CA6 and that at the AA7a extending to AA8 appear to be similar to that at CA3a extending to CA4 (in unit cell B). The height profile along L6 is also found to be similar to that along L3. However, the corresponding height profile along L5 appears different from that of L4 due to the presence of the adsorption at AA7a. The filled-state image for unit cell C shows that the adsorption of the glycine moieties at CA5a and at AA7a evidently has caused H adsorption at the respective neighboring restatoms RA5d and RA7d. The H adsorption is illustrated by the missing intensity at these restatom locations, RA5d and RA7d, and the concomitant increase in intensities of the neighboring adatoms (AA5b and CA5c for RA5d, and CA7b and CA6 for RA7d). The higher intensity for AA5b is quite apparent in the height profile along line scan L16, when compared to L12 along the unreacted sites. The intensity increase at CA6 caused by H adsorption at RA7d due to electron redistribution also partially counters the intensity reduction at CA6 due to adsorption at CA5a (as similarly observed for the CA3a, CA4 pair in unit cell B). The near-normal intensity for CA6 therefore suggests a more vertically oriented glycine fragment adsorbed at the CA5a site, when compared to that at the CA3a site. This upright unidentate adsorption geometry, as also obtained by our DFT calculation, has been discussed in our earlier XPS study.[21] Furthermore, the adsorption at corner adatom AA7a has also caused intensity depletion at the corner adatom AA8 across the dimer wall, when compared to the unreacted corner adatoms of the same half unit cell. This is consistent with the presence of weak dipole−dipole-like interaction between the glycine fragment at AA7a and the adatom across the dimer wall (AA8), as proposed earlier as in the case of the CA3a, CA4 pair. In addition, the deep trough found in the height profile along line scan L15 can be attributed to both the H adsorption at RA7d and the glycine fragment adsorption at AA7a.

In order to investigate the reactivity of different sites on Si(111)7×7 toward glycine, we show, in Figure 2, the empty-state images, collected with a tunneling current of 200 pA at a sample bias of +2 V, for five different glycine exposures. As demonstrated in Figure 1, a protrusion in an empty-state image can be used reliably to indicate a glycine fragment adsorbed on a surface site, in contrast to the more complex variation in filled-state images. Using an image size of 50 × 50 nm^2 (with approximately 400 complete unit cells), as shown, for example, for the 35 s exposure in Figure 2e, we determine the relative occupancies of the different sites (i.e., CA vs AA) and of the sites on the faulted and unfaulted half unit cells, as well as the total coverage (i.e., the fraction of the available sites that are occupied by glycine fragments). To obtain the relative occupancies of sites in the faulted and unfaulted half unit cells, we have also taken appropriate account of the corresponding filled-state images (not shown). To better illustrate the adsorption features, we show, in Figure 2a−d, only 17 × 17 nm^2 sections of the complete 50 × 50 nm^2 images (that we use for our statistical analysis). Not surprisingly, the total coverage of adsorbed glycine fragments is found to be increasing linear with increasing exposure time in the early growth stage considered here (Figure 2f). In accord with dissociative adsorption of glycine on one of six adatoms in a half unit cell, for which the dissociated H atoms would occupy one of the three restatoms in the half unit cell, the maximum number of glycine adsorption in a half unit is therefore three, making the maximum possible total coverage to be 0.5 monolayer (where we define a monolayer coverage as the total number of Si adatom sites). Closer examination of the empty- and filled-state images shows that the relative occupancy for the CA sites is higher than that of AA for each of the exposures (Figure 2f), in good accord with the fact that the CA sites are more electrophilic[26] and therefore more reactive to glycine than the AA sites. Furthermore, the relative occupancies of CA and of AA increase linearly with exposures, with the CA occupancy lying ∼30% higher than the AA occupancy. In particular, the ratio between the relative occupancies for AA and CA is found to increase from 0.61 for the 8 s exposure to 0.66 for 20 s exposure and to 0.73 for 35 s exposure, which indicates that the rate of increase of adsorption on the AA sites increases faster than that on the CA sites with increasing exposure. The presence of a higher proportion of the unreacted AA sites than the unreacted CA sites is consistent with the earlier saturation of the CA sites before that of AA sites with increasing exposure. In addition, the majorities of the occupied CA sites (from a relative occupancy of 54% for 8 s to 50% for 35 s) and AA sites (from a relative occupancy of 26% for 8 s to 23% for 35 s) are found on the faulted half. This is consistent with the higher occupancy of sites on the faulted half than that on the unfaulted half, with the ratio between the relative occupancies for unfaulted half and faulted half found to increase from 0.21 for the 8 s exposure to 0.32 for 20 s exposure and to 0.49 for 35 s exposure. The observed earlier saturation of the faulted half sites than the unfaulted half sites with increasing exposure is consistent with the higher reactivity of sites on the faulted half toward glycine. The CA (AA) sites on the faulted (unfaulted) half are therefore the most (least) reactive toward glycine adsorption.

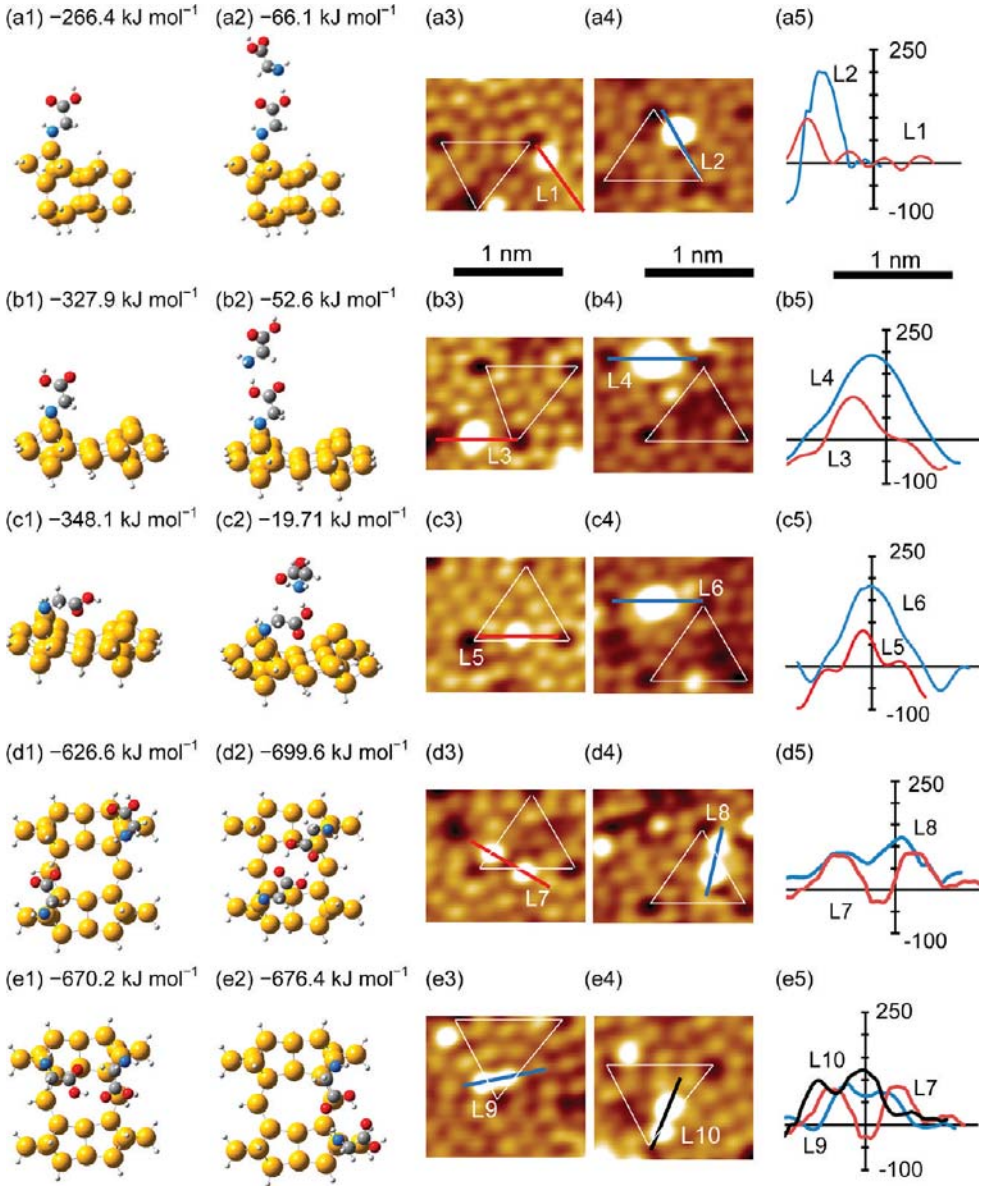

Figure 3. Equilibrium structures and the adsorption energies of glycine on (a1, a2) $Si_{16}H_{18}$ and (b1−e1, b2−e2) $Si_{26}H_{24}$ in (a1−d1) the single and (a2−d2, e1, e2) double configurations, with the configurations for parts d1, d2, e1, and e2 shown as the top view, all obtained with DFT/B3LYP/6-31G++(d,p). STM images taken at a sample bias of +2 V and a tunneling current of 200 pA attributed to the corresponding (a3−d3) single and (a4−d4, e3, e4) double configurations, with the height profiles along the respective linescans (L1−L10) given in parts a5−e5. The corresponding adsorption energies of glycine for the single and horizontal double configurations are indicated in parts a1−c1 and d1, e1, d2, e2, respectively. The hydrogen bond energies of the vertical double configurations, as estimated by differences between their adsorption energies and those of their corresponding singles plus a free glycine molecule, are given in parts a2−c2.

The STM images in Figure 2 also reveal that while a predominant number of glycine molecules adsorbed individually (singles) appear as protrusions of similar size, some of the protrusions, marked by open squares in Figure 2, are discernibly larger (by at least 30% in diameter). As illustrated in Figure 3, these larger protrusions could be identified as an adsorbed glycine fragment vertically attached to a second glycine molecule by H-bonding (vertical doubles). Furthermore, glycine molecules also appear to adsorb in pairs in neighboring sites, which could be the result of two adsorbed glycine fragments horizontally attached to each other by H-bonding (horizontal doubles). If we consider that the most probable adsorption were to occur at a center adatom site such as CA1 in the upper part of Figure 1c (unit cell A), then a second glycine adsorption at CA2 (with a separation of 6.65 Å from CA1), at AA9a, CA9b, CA9c, or AA9d (each with a separation of 7.68 Å from CA1), as well as at AA9e or AA9f (each with a separation of 10.15 Å from CA1) could form the horizontal doubles (marked as open eclipses in Figure 2). However, since the adsorption at CA1 would affect the LDOS at CA2, as discussed earlier, the second glycine adsorption on the other neighboring sites would be more likely. As shown in Figure 2f, the relative occupancy (with respect to the total number of available sites) for the horizontal doubles (HD) is found to be consistently larger than that of the vertical doubles (VD). As the exposure time increases, both relative occupancies

dx.doi.org/10.1021/jp300011k | J. Phys. Chem. C 2012, 116, 10968−10975

for VD and HD increase, with a higher increase in the VD occupancy at a higher exposure. These trends are consistent with the random statistical nature of molecular collisions with the surface in the adsorption process. It is also not surprising that the relative occupancies for HD and VD are considerably smaller than those of the singles during the initial stage of adsorption.

To understand the nature of the VD and HD adsorption mediated by H-bonding, we perform ab initio calculations based on the DFT with a B3LYP hybrid functional[35,36] and a 6-31G++(d,p) basis set using the Gaussian 09 software.[37] To simulate the adsorption of a single glycine molecule on the 7×7 surface, we employ the $Si_{16}H_{18}$ and $Si_{26}H_{24}$ clusters to provide model surfaces for the adatom−restatom pair and the two adjacent adatom−adatom pairs across the dimer wall, respectively. In our earlier XPS study,[21] we have demonstrated that glycine undergoes initial N−H dissociative adsorption and formation of a transitional layer mediated by the [−H_2N···HO(O)C−] H-bonds. The adsorption energies of the corresponding adsorbate−substrate configurations (ASCs) for "upright" single adsorption on the adatom−restatom pair (Figure 3a1, −266.4 kJ mol^{-1}) and the double adatom−adatom pairs across the dimer wall (Figure 3b1, −327.9 kJ mol^{-1}) are found to be in a similar energy range as the "tilted" single adsorption on the double adatom−adatom pairs across the dimer wall (−348.1 kJ mol^{-1}, Figure 3c1), after consideration of the different clusters employed for modeling the different substrate sites. By adding a glycine molecule to the respective single ASCs in an appropriate fashion, we obtain the upright VD (Figures 3a2, 3b2) and tilted VD ASCs (Figure 3c2). The differences between the adsorption energies of upright and tilted VD ASCs and those of its corresponding singles plus a free glycine molecule give an estimation of the hydrogen bond energies, which are respectively −66.1 kJ mol^{-1} (a2), −52.6 kJ mol^{-1} (b2), and −19.79 kJ mol^{-1} (c2). Interestingly, except for the tilted VD (c2), these values are found to be comparable to those calculated for [−H_2N···HO(O)C−] (−48.5 kJ mol^{-1}) and [−C(OH)O···HO(O)C−] H-bonds (−67.6 kJ mol^{-1}) in free glycine molecules. For the tilted VD (c2), the weaker hydrogen bond strength is likely due to poor molecular alignment between the participating molecules.

Parts a3−c3 and a4−c4 of Figure 3 show typical STM images of these upright and tilted single and VD ASCs, respectively, with their corresponding height profiles along selected line scans shown in Figure 3a5−c5. In particular, as shown in Figure 3a5, the maximum height along L2 (200 pm) of the upright VD at the AA site (Figure 3a4) is nearly twice that along L1 (100 pm) of the upright single at the AA site (Figure 3a3). A similar height difference (Figure 3b5) is also observed along L4 for the upright VD at the CA site (200 pm, Figure 3b4), relative to that along L3 for the corresponding upright single (100 pm, Figure 3b3). The nearly twice height differences between the upright VD and their corresponding singles confirm the presence of the second glycine molecule H-bonded to their respective singles. For the tilted single at the CA site (Figure 3c3), the maximum height along L5 (80 pm, Figure 3c5) is discernibly less than that along L3 (100 pm, Figure 3b5) of the upright single at the CA site (Figure 3b3), which is consistent with the upright and tilted geometries in the respective ASCs. Similarly, the maximum height along L6 (180 pm, Figure 3c5) for the titled VD at the CA site (Figure 3c4) is also found to be smaller than that along L4 (200 pm, Figure 3b5) for the vertical VD at the CA site, which again is consistent with the proposed tilted VD ASC (Figure 3c2). The degree of tilt depends on the extent of the dipole−dipole interaction between the COOH terminus and the unreacted adatom across the dimer wall and could extend from vertical (no interaction) to near-horizontal (maximum interaction).

The STM image of two independent singles at a CA site and an adjacent AA site diagonally across the dimer wall (Figure 3d3) exhibits a height profile along the diagonal L7 with maximum height (80 pm) similar to that of a tilted single (Figure 3c3, L5). For the STM image of a typical HD (Figure 3d4), the height profile along the diagonal L8 (Figure 3d5) clearly shows similar maximum height as that of the two independent singles but with smaller separation between their peak maxima, which confirms the formation of H-bonding. Furthermore, the STM images of other HDs (Figure 3e3, 3e4) also exhibit similar height profiles along L9 and L10 (Figure 3e5) as that along L8 (Figure 3d5), which illustrates the variety of possible HD arrangement for different adjacent sites. Our DFT calculation shows an example of an ASC with two glycine fragments independently adsorbed at adatoms diagonally across the dimer wall, with different degrees of tilt (Figure 3d1). Our calculation also shows the formation of HD ASCs mediated by double H-bonding between two COOH termini from the glycine fragments adsorbed on adatoms diagonally across (Figure 3d2), on the same side of (Figure 3e1), and directly across the dimer wall (Figure 3e2).

4. CONCLUSIONS

The early adsorption of glycine on Si(111)7×7 has been studied by STM. At the initial stage of adsorption (low exposure), we observe empty- and filled-state images that correspond predominantly to individual (or single) H-dissociative adsorption of glycine at an adatom−restatom pair on the 7×7 surface. Of particular interest is the observation that the unidentate adsorption also affects the LDOS on the complementary adatom site (across the dimer wall), consequently reducing its occupancy. At a higher exposure, larger protrusions could be observed and identified by height profile analysis as an adsorbed glycine fragment vertically attached to a second glycine molecule by H-bonding. This is in good accord with our earlier XPS study that shows N−H dissociative adsorption of glycine and the formation of a transitional layer mediated by the [−H_2N···H−OC(O)−] H-bonding. Furthermore, adsorption in pairs in adjacent sites could also be found and attributed to two adsorbed glycine fragments horizontally attached to each other by H-bonding. The present work therefore demonstrates, for the first time, the presence of [−(OH)C═O···H−OC(O)−] H-bonding in the formation of the interfacial (or first) adlayer. We also illustrate the plausibility of these single and H-bonding-mediated vertical and horizontal double adsorption configurations by DFT/B3LYP calculations involving model surfaces of $Si_{16}H_{18}$ and $Si_{26}H_{24}$ clusters. Statistical analysis of STM images collected at different exposures further reveals that the apparent reactivity of individual sites toward glycine decreases in the following order: CA on the faulted half > AA on the faulted half > AA on the unfaulted half > CA on the unfaulted half. In the early stage of adsorption considered in the present work, the relative occupancies of these respective sites exhibit a linear trend, with the more reactive sites saturated faster than the less reactive ones. Furthermore, the relative occupancies for the horizontal doubles are notably larger than that of the vertical

doubles, with the singles significantly larger than the doubles in this early adsorption stage.

AUTHOR INFORMATION

Corresponding Author

*E-mail: tong@uwaterloo.ca.

Notes

The authors declare no competing financial interest.

ACKNOWLEDGMENTS

This work was supported by the Natural Sciences and Engineering Research Council of Canada.

REFERENCES

(1) Chen, Q.; Frankel, D. J.; Richardson, N. V. *Langmuir* **2002**, *18*, 3219−3225.
(2) Frankel, D. J.; Chen, Q.; Richardson, N. V. *J. Chem. Phys.* **2006**, *124*, 204704.
(3) Chen, Q.; Frankel, D. J.; Richardson, N. V. *Surf. Sci.* **2002**, *497*, 37−46.
(4) Lofgren, P.; Krozer, A.; Lausmaa, J.; Kasemo, B. *Surf. Sci.* **1997**, *370*, 277−292.
(5) Huang, J. Y.; Ning, Y. S.; Yong, K. S.; Cai, Y. H.; Tang, H. H.; Shao, Y. X.; Alshahateet, S. F.; Sun, Y. M.; Xu, G. Q. *Langmuir* **2007**, *23*, 6218−26.
(6) Strother, T.; Cai, W.; Zhao, X.; Hamers, R. J.; Smith, L. M. *J. Am. Chem. Soc.* **2000**, *122*, 1205−1209.
(7) Oliveira Brett, A. M.; Chiorcea, A.-M. *Langmuir* **2003**, *19*, 3830−3839.
(8) Gray, J. J. *Curr. Opin. Struct. Biol* **2004**, *14*, 110−5.
(9) Seker, F.; Meeker, K.; Kuech, T. F.; Ellis, A. B. *Chem. Rev* **2000**, *100*, 2505−36.
(10) Ashkenasy, G.; Cahen, D.; Cohen, R.; Shanzer, A. *Acc. Chem. Res.* **2002**, *35*, 121−128.
(11) Wolkow, R. A. *Annu. Rev. Phys. Chem.* **1999**, *50*, 413.
(12) Vilan, A.; Shanzer, A.; Cahen, D. *Nature* **2000**, *404*, 166−8.
(13) Heath, J. R. *Annu. Rev. Mater. Res.* **2009**, *39*, 1−23.
(14) Hamley, I. W. *Angew. Chem., Int. Ed.* **2003**, *115*, 1730−1752.
(15) Venugopal, V.; Chatterjee, A.; Ebrahimi, M.; He, Z. H.; Leung, K. T. *J. Chem. Phys.* **2010**, *132*, 174702.
(16) Kawasaki, T.; Sakai, D.; Kishimoto, H.; Akbar, A. A.; Ogawa, T.; Oshima, C. *Surf. Interface Anal.* **2001**, *31*, 126−130.
(17) Yuan, Z. L.; Chen, X. F.; Wang, Z. H.; Yong, K. S.; Cao, Y.; Xu, G. Q. *J. Chem. Phys.* **2003**, *119*, 10389.
(18) Tanaka, K.-I.; Xie, Z.-X. *J. Chem. Phys.* **2005**, *122*, 54706.
(19) Baik, J.; Kim, M.; Park, C.-Y.; Kim, Y.; Ahn, J. R.; An, K.-S. *J. Am. Chem. Soc.* **2006**, *128*, 8370−1.
(20) Cao, X.; Hamers, R. J. *J. Am. Chem. Soc.* **2001**, *123*, 10988−96.
(21) Zhang, L.; Chatterjee, A.; Ebrahimi, M.; Leung, K. T. *J. Chem. Phys.* **2009**, *130*, 121103.
(22) Lopez, A.; Heller, T.; Bitzer, T.; Richardson, N. V. *Chem. Phys.* **2002**, *277*, 1−8.
(23) Qu, Y.; Wang, Y.; Li, J, W.; Han, K.-L. *Surf. Sci.* **2004**, *569*, 12−22.
(24) Chatterjee, A.; Zhang, L.; Leung, K. T. *Chem. Phys. Lett.* **2011**, *508*, 219−223.
(25) Nyberg, M.; Hasselström, J.; Karis, O.; Wassdahl, N.; Weinelt, M.; Nilsson, A.; Pettersson, L. G. M. *J. Chem. Phys.* **2000**, *112*, 5420.
(26) Waltenburg, H. N.; Yates, J. T. *Chem. Rev* **1995**, *95*, 1589−1673.
(27) Northrup, J. E. *Phys. Rev. Lett.* **1986**, *57*, 154−157.
(28) Tao, F.; Xu, G. Q. *Acc. Chem. Res.* **2004**, *37*, 882−93.
(29) Cao, Y.; Yong, K. S.; Wang, Z. H.; Deng, J. F.; Lai, Y. H.; Xu, G. Q. *J. Chem. Phys.* **2001**, *115*, 3287.
(30) Tao, F.; Wang, H. W.; Xu, G. Q. *Surf. Sci.* **2003**, *530*, 203−215.
(31) Feenstra, R. M. *Surf. Sci.* **1994**, *299−300*, 965−979.
(32) Lo, R.-L.; Ho, M.-S.; Hwang, I.-S.; Tsong, T. *Phys. Rev. B* **1998**, *58*, 9867−9875.
(33) Boland, J. *Surf. Sci.* **1991**, *244*, 1−14.
(34) Lo, R.-L.; Hwang, I.-S.; Ho, M.-S.; Tsong, T. *Phys. Rev. Lett.* **1998**, *80*, 5584−5587.
(35) Becke, A. D. *J. Chem. Phys.* **1993**, *98*, 5648.
(36) Lee, C.; Yang, W.; Parr, R. G. P. *Phys. Rev. B* **1988**, *37*, 785.
(37) Frisch, M. J.; et al. *Gaussian 09 2009*; Gaussian Inc.: Wallingford CT, 2009.